Asian Journal of Chemistry; Vol. 37, No. 9 (2025), 2195-2201
ASIAN JOURNAL OF CHEMISTRY
https://doi.org/10.14233/ajchem.2025.34252

Unveiling the Analysis of Gd^{3+} Doping on Structural, Compositional and Morphological Studies of $Zn_{0.5}Mg_{0.5}Gd_xFe_{(2-x)}O_4$ Ferrites

GHEWAR RAM[1,*], UMMED SINGH[1], SAHI RAM[1], HIMANSHU[2,3] and DEEPAK SUTHAR[4]

[1]Department of Physics, Jai Narain Vyas University, Jodhpur-342005, India
[2]Department of Physics, University Institute of Sciences, Chandigarh University, Mohali-140413, India
[3]University Centre for Research & Development, Chandigarh University, Mohali-140413, India
[4]Hangzhou International Innovation Institute of Beihang University, Hangzhou 311115, P.R. China

*Corresponding author: E-mail: ghewarchoudhary2025@gmail.com

Received: 14 June 2025 *Accepted*: 31 July 2025 *Published online*: 30 August 2025 AJC-22099

This study reports the structural, morphological and compositional properties of a series of gadolinium doped $Zn_{0.5}Mg_{0.5}Gd_xFe_{(2-x)}O_4$ ferrites where x = 0.0, 0.04, 0.08 and 0.12. The ferrites were synthesized using a co-precipitation method and their properties were analyzed using X-ray diffraction (XRD), scanning electron microscopy (SEM) and Fourier transform infrared spectroscopy (FT-IR). The XRD results showed that the ferrites had both cubic and tetragonal spinal structures. The lattice constants and crystallite sizes of the ferrites were found to vary with the Gd^{3+} substitution level. The SEM images revealed that the ferrites consisted of nanoparticles of varying sizes and shapes, exhibiting a certain level of agglomeration. The FT-IR spectra confirmed the presence of characteristic M–O vibrations, indicating the successful formation of ferrite structures. These results suggest that the structural and morphological properties of Gd-doped $Zn_{0.5}Mg_{0.5}Gd_xFe_{(2-x)}O_4$ can be tailored by adjusting the Gd^{3+} substitution level.

Keywords: Gd doping, Structural study, Compositional study, Ferrites.

INTRODUCTION

Spinel ferrite is a magnetic oxide material with high DC resistance, high chemical stability, low cost, mechanical hardness, low porosity, easy synthesis, high magnetic permeability and high magnetic field [1-5]. These materials have attracted the attention of the scientific community and have been used in many applications such as storage devices, transformer cores, magnetic sensors, satellite communication, fuel sensors, computer components and magnetic refrigerators. Magnetocaloric effect occurs in spinel ferrite materials when the order of the magnetic moment changes due to changes in magnetic properties [6-8]. The change in the order of the spinel ferrite magnetic material causes cooling by absorbing heat from the system to be energized.

In order to keep the process cool, the magnetic ordering temperature (MOT) must be reduced to room temperature [9,10]. The physical and chemical properties of different metal cations are affected by their type, amount and location [11-14]. Magnesium ferrite is used as a humidity sensor and catalyst [15]. Super paramagnetic ferrites are attractive for biomedical applications, especially in magnetic carrier technology [16-18]. They have strong magnetic properties, excellent chemical stability, corrosion resistance and high resistivity. Their crystal structure, chemical elements and physical properties make them of interest from both theoretical and practical points of view [19,20]. The specific magnetic moment of Gd^{3+} ions, generated by seven different generators, works like a powerful switch, allowing scientists to optimally tune the properties of ferrites. This opens up valuable resources for the creation of new electronic products with good technical properties. Among the spinel ferrite family, Gd-doped Zn-Mg ferrites stand out as particularly intriguing materials [21-23]. The unique magnetic moment of Gd^{3+} ions, arising from their seven unpaired electrons, acts as a potent tuning knob, allowing researchers to tailor the properties of these ferrites with exquisite precision. This opens up a treasure trove of possibilities for designing novel magneto-electric materials with functionalities specifically tailored for cutting-edge technological applications. The captivating world of Gd-doped Zn-Mg

ferrites, specifically focusing on the $Zn_{0.5}Mg_{0.5}Gd_xFe_{(2-x)}O_4$ system, is the heart of this research. We utilize a co-precipitation technique, a well-established method renowned for its simplicity and control over particle size and morphology, to bring these fascinating materials to life.

EXPERIMENTAL

The high grade requisite chemicals like zinc nitrate hexahydrate [$Zn(NO_3)_2·6H_2O$], magnesium nitrate hexahydrate [$Mg(NO_3)_2·6H_2O$, ferric nitrate nonahydrate [$Fe(NO_3)_3·9H_2O$], gadolinium nitrate hexahydrate [$Gd(NO_3)_3·5H_2O$], ammonia solution (NH_4OH) for the pH adjustment were procured from different commercial sources.

Synthesis: The Gd-doped $Zn_{0.5}Mg_{0.5}Gd_xFe_{(2-x)}O_4$ was synthesized by co-precipitation method. For synthesis of ferrites, $Fe(NO_3)_3·9H_2O$, $Zn(NO_3)_2·6H_2O$, $Mg(NO_3)_2·6H_2O$ and $Gd(NO_3)_3·5H_2O$ were first dissolved in 300 mL of distilled water while preserving a 2:1 ratio. The precipitation procedure was started by adding a 1 M NaOH solution dropwise while stirring continuously until the pH of the solution reached 10. The resultant precipitates were then washed by centrifugation with acetone and distilled water. The precipitates were then separated by filtering using a Büchner funnel. The precipitates were then dried in an oven at 80 ºC for around 24 h to remove any moisture. The sample was then ground and crushed from the dry residue to develop a fine powder. This powder was calcined in order to complete the synthesis.

Characterization: The structural characterization of Gd-doped $Zn_{0.5}Mg_{0.5}Gd_xFe_{(2-x)}O_4$ (x = 0.0, 0.04, 0.08 and 0.12%) ferrites was performed using an X-ray diffractometer equipped with Cu*K*α radiation (λ = 1.5418 Å). The morphological studies of pure and doped ferrites were performed with a scanning electron microscope (SEM). The absorption peaks in the wavenumber range of 4000-400 cm^{-1} were measured by FT-IR spectrometer (make: NiCOLETIS5).

RESULTS AND DISCUSSION

Structural analysis: Fig. 1 shows the X-ray diffraction (XRD) patterns of gadolinium-doped $Zn_{0.5}Mg_{0.5}Gd_xFe_{(2-x)}O_4$ powder with different concentrations of gadolinium (x = 0.0, 0.04, 0.08 and 0.12%) and samples were named G_0, G_1, G_2 and G_3, respectively. For all the samples, there are diffraction peaks at (220), (311), (400), (422), (511) and (440) with different intensity. The absence of impurity peaks suggests that the samples are chemically pure, showing no signs of foreign materials or unwanted byproducts. This indicates that the synthesis or purification process was successful, yielding a high-quality material appropriate for further examination. The samples have a cubic spinel structure with *Fd*3*m* space group and also a tetragonal spinel structure with $I4_1/$and space group [1]. These peaks were perfectly matched with the standard JCPDS card No. 73-1963 and ICDD# (00-034-0425) [24-26]. The interplanar spacing (d) and crystalline size (D) were calculated through Bragg's and Scherrer formulae, respectively as under:

$$d = \frac{\lambda}{2\sin\theta} \quad (1)$$

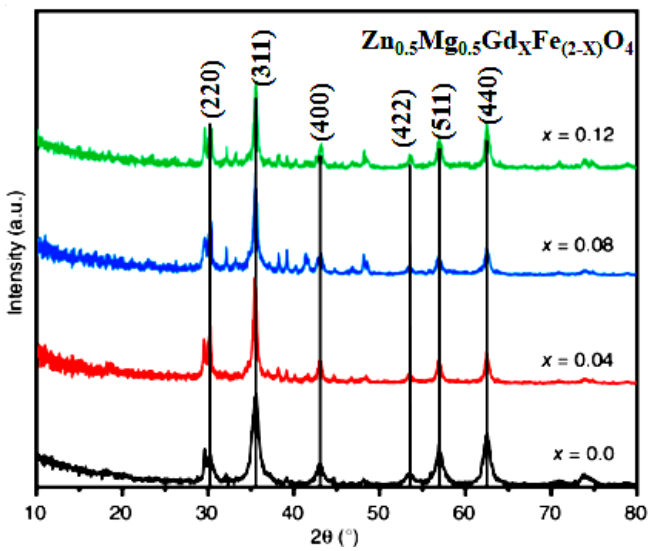

Fig. 1. XRD patterns of $Zn_{0.5}Mg_{0.5}Gd_xFe_{(2-x)}O_4$ (x = 0.0, 0.04, 0.08 and 0.12) ferrites

$$D = \frac{0.94\lambda}{\beta\cos\theta} \quad (2)$$

here 'λ' is the wavelength of the X-rays; β is the full width at half maximum and θ is half-angle between the incident and scattered X-rays. The interplanar spacing found to be varied with the increasing the Gd content (x) as well as the grain size is increased as 15 nm, 16 nm, 17 nm and 17 nm with different concentrations of gadolinium (x = 0.0, 0.04, 0.08 and 0.12%), respectively. The lattice constant (a) for cubic phase is determined by the formula concerned as below:

$$\frac{1}{d^2} = \frac{h^2 + k^2 + l^2}{a^2} \quad (3)$$

where *hkl* denotes the Miller Indices.

The dislocation density (δ) and micro-internal strain (ε) were calculated the corresponding to preferred orientation by following respective equations:

$$d = \frac{1}{D^2} \quad (4)$$

$$\varepsilon = \frac{\beta}{4\tan\theta} \quad (5)$$

When Gd^{3+} ions were added to the $Zn_{0.5}Mg_{0.5}Fe_2O_4$, the size of the crystal lattice increases as the amount of gadolinium increases. This effect is due to the larger size of Gd^{3+} ions, which have an ionic radius of 0.938 Å, in contrast to Fe^{3+} ions with a radius of 0.645 Å. When more Gd^{3+} ions are added, they take up more space in the crystal lattice, making the overall structure bigger [27]. The lattice constant exhibits an initial increase with gadolinium doping, followed by a decrease beyond x = 0.8, attributed to the limited solubility of gadolinium and its larger ionic radius. The XRD patterns reveal a shift in peak positions with increasing gadolinium content, indicating variations in the lattice parameters. Another reason for the increase in the lattice constant is the substitution of rare earth elements, the same trend is also reported in an earlier study on rare earth doped Zn-Mg ferrites [28]. The substitution of smaller iron ions (0.645 Å) with larger Gd^{3+} ions (1.01 Å) in the magnesium ferrite structure leads to an

initial increase in the lattice constant, but this expansion is limited beyond $x = 0.8$ due to the limited solubility of gadolinium [23]. The Williamson-Hall (W-H) relation (given in eqns. 6-8) relates the mean crystallite size and micro-strain to the broadening of diffraction peak where the crystallite size is calculated using eqn. 8:

$$\beta_{2\theta} = \frac{0.94\lambda}{D\cos\theta} + 4\varepsilon\tan\theta \quad (6)$$

$$\beta_{2\theta}\cos\theta = \frac{K\lambda}{D} + 4\varepsilon\sin\theta \quad (7)$$

$$\text{Crystallite size (D)} = \frac{k\lambda}{\text{Intercept}} \quad (8)$$

here, $\beta_{2\theta}$ is the full width at half-maximum (FWHM) and D is crystallite size, ε is the root mean square value of the micro-strain. The parameter k (0.9-1) is the shape factor for spherical crystallite size. The crystallite size can be calculated by using the intercept and strain using the slope of straight lines (curves between $\beta_{2\theta}\cos\theta$ *versus* $4\sin\theta$) or Williamson-Hall plots as shown in Fig. 2. The crystallite size is increased with different concentrations of gadolinium (x = 0.0, 0.04, 0.08 and 0.12%) respectively. The positive slope of these plots indicates a lattice expansion, whereas the negative slope indicates a lattice compression. All the calculated structural parameters are shown in Table-1.

Surface morphological analysis: SEM analysis was also employed to explain the effect of gadolinium doping on the morphology of synthesized Gd-doped Zn-Mg ferrites. A SEM image of $Zn_{0.5}Mg_{0.5}Gd_xFe_{(2-x)}O_4$ is shown in Fig. 3, which revealed that the prepared ferrites have a comparatively rod morphology and the non-homogeneity among the particle sizes of the sample. The voids present in the samples are a result of the escape of some gases during the evaporation procedure. It was also found that the particles obtained by the co-precipitation method are slightly agglomerated. The crystalline size was found to be < 38 nm.

The particle size distribution bar graphs of Gd-doped Zn-Mg ferrites having different Gd concentrations is presented in Fig. 4. The grain size was calculated with the help of Image J open access software and obtained grain size is 44 nm, 31 nm, 33 nm and 20 nm for $Zn_{0.5}Mg_{0.5}Gd_xFe_{(2-x)}O_4$ (x = 0.00, 0.04, 0.08, 0.12).

FTIR studies: As shown in Fig. 5, it was observed that in case of pure $ZnMgFe_2O_4$ (G_0), the peaks in the range of 600 to 400 cm^{-1} due to the Zn–O, Mg(II)–O and Fe(III)–O

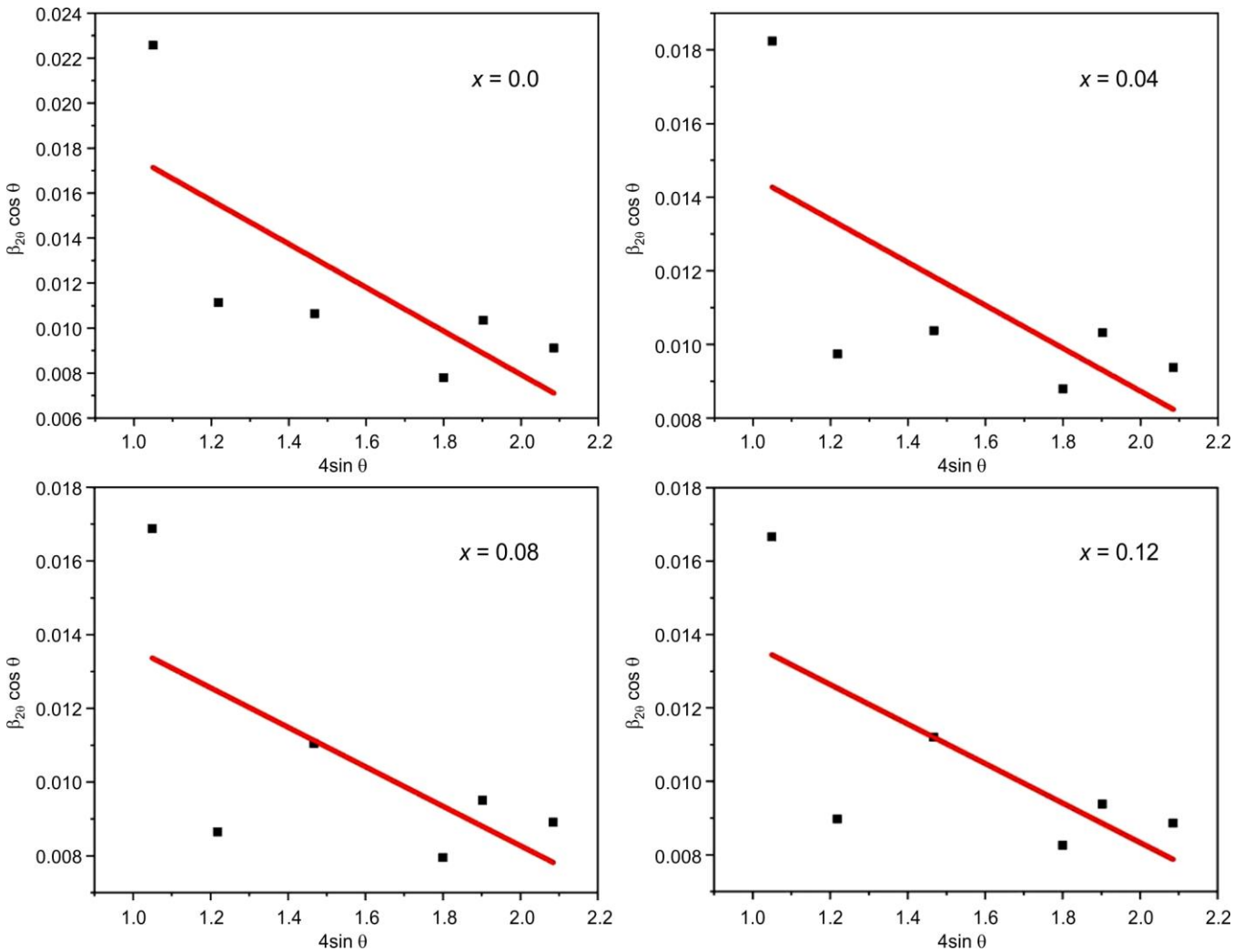

Fig. 2. Williamson-Hall plots of $Zn_{0.5}Mg_{0.5}Gd_xFe_{(2-x)}O_4$ (x = 0.0, 0.04, 0.08 and 0.12) ferrites

TABLE-1
XRD PARAMETERS VALUES OF $Zn_{0.5}Mg_{0.5}Gd_xFe_{(2-x)}O_4$ (x = 0, 0.04, 0.08 AND 0.12) FERRITES

Gd content (x)	2θ (º)	*hkl*	d (Å)	a (Å)	Intercept	W-H D (nm)	Scherrer D (nm)	$\varepsilon \times 10^{-3}$	$\delta \times 10^{15}$ (m^{-2})
0	17.76	311	0.498	1.64	0.02729	5	15	1.15	4.19
0.04	17.73	311	0.499	1.65	0.02039	7	16	1.50	4.08
0.08	17.74	311	0.499	1.65	0.01899	8	17	1.40	3.57
0.12	17.78	311	0.498	1.64	0.01910	8	17	1.39	3.52

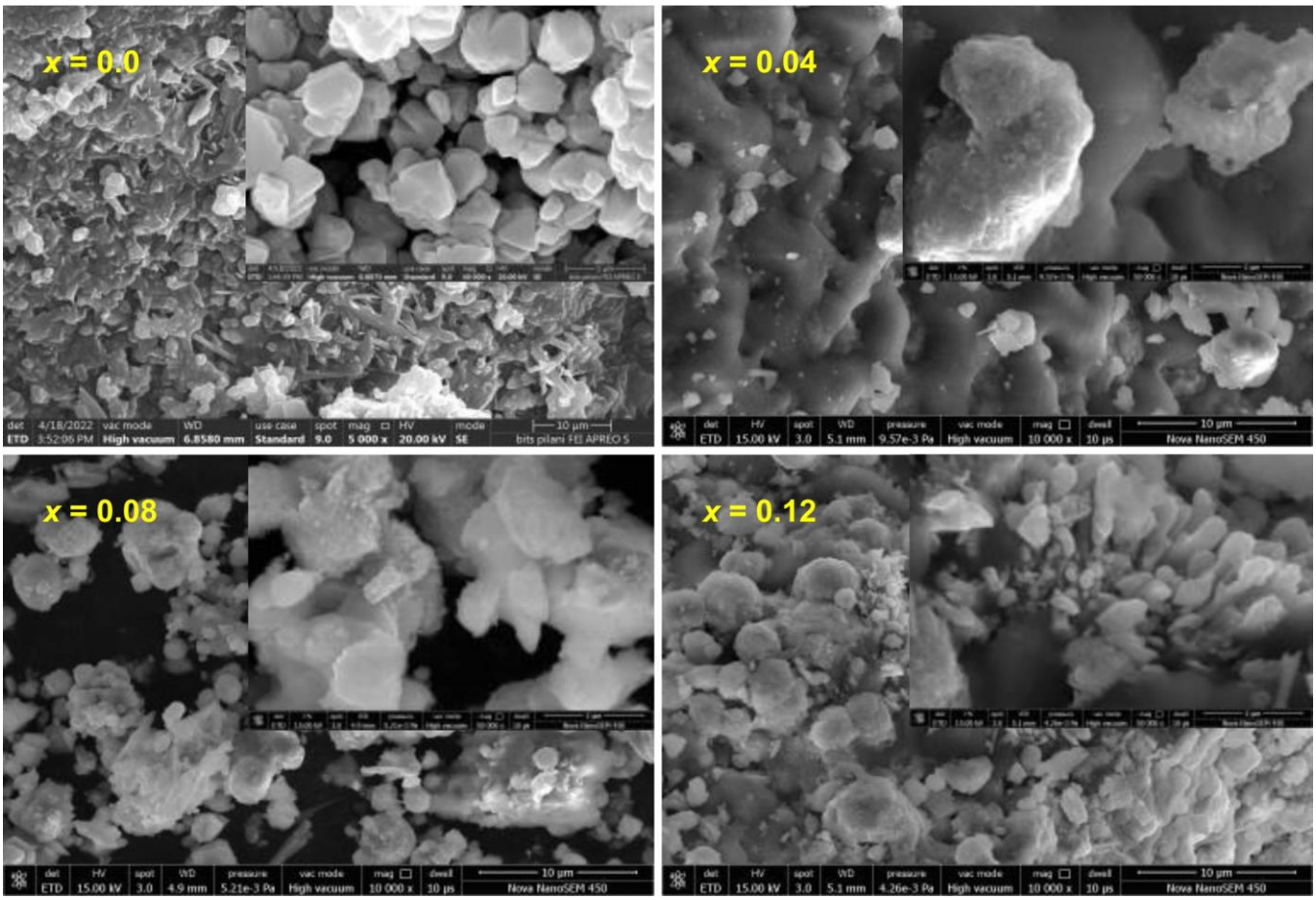

Fig. 3. Surface morphological micrographs of $Zn_{0.5}Mg_{0.5}Gd_xFe_{(2-x)}O_4$ (x = 0.0, 0.04, 0.08 and 0.12) ferrites

bond of spinel-type oxide [29,30]. The highest intensity band that appears between 600-400 cm^{-1} is the characteristic of the stretching of the Zn-O bond in wurtzite structures, the most common crystalline form of the oxide. The lower intensity peak is observed at 670 cm^{-1} is also characteristic of the stretching of the Zn-O bonds for all the samples [31]. The bands appearing at ~1000, ~850 and ~750 cm^{-1} correspond to the stretching vibrations of Zn–O bonds, characteristic of tetrahedral coordination region. In the region around the wavelength of 3500 cm^{-1}, a band of low intensity is observed, which can be attributed to the stretching of O-H bonds, which have already been observed in studies involving materials of the same nature and which are generally related to water absorbed by the surface in the analysis [32].

Vibrating sample magnetometer (VSM) analysis: The saturation magnetization (M_s), remanent magnetization (M_r), coercivity (H_c) and hysteresis loop area are the key magnetic parameters that characterize the behaviour of magnetic materials. Three different samples were analyzed, with the Gd_3 sample exhibiting the highest values for M_s, M_r, H_c and hysteresis loop area as compared to the Gd_2 and Gd_1 samples (Fig. 6). The saturation magnetization (M_s) represents the maximum magnetization that a material can achieve in an applied magnetic field. In this study, the Gd_3 sample had an estimated M_s of approximately 18 emu/g, while the Gd_2 and Gd_1 samples had lower values of 12 emu/g and 9 emu/g, respectively. The remanent magnetization (M_r) refers to the residual magnetization left in the material when the external magnetic field is reduced to zero. The Gd_3 sample exhibited a higher M_r of around 6 emu/g compared to the Gd_2 and Gd_1 samples, which had values of 4 emu/g and 3 emu/g, respectively. This suggests that the Gd_3 sample retains more magnetization after the external field is removed.

Coercivity (H_c) is the magnetic field required to reduce the magnetization to zero after the material has been magnetized. The Gd_3 sample had a higher coercivity of approxi-

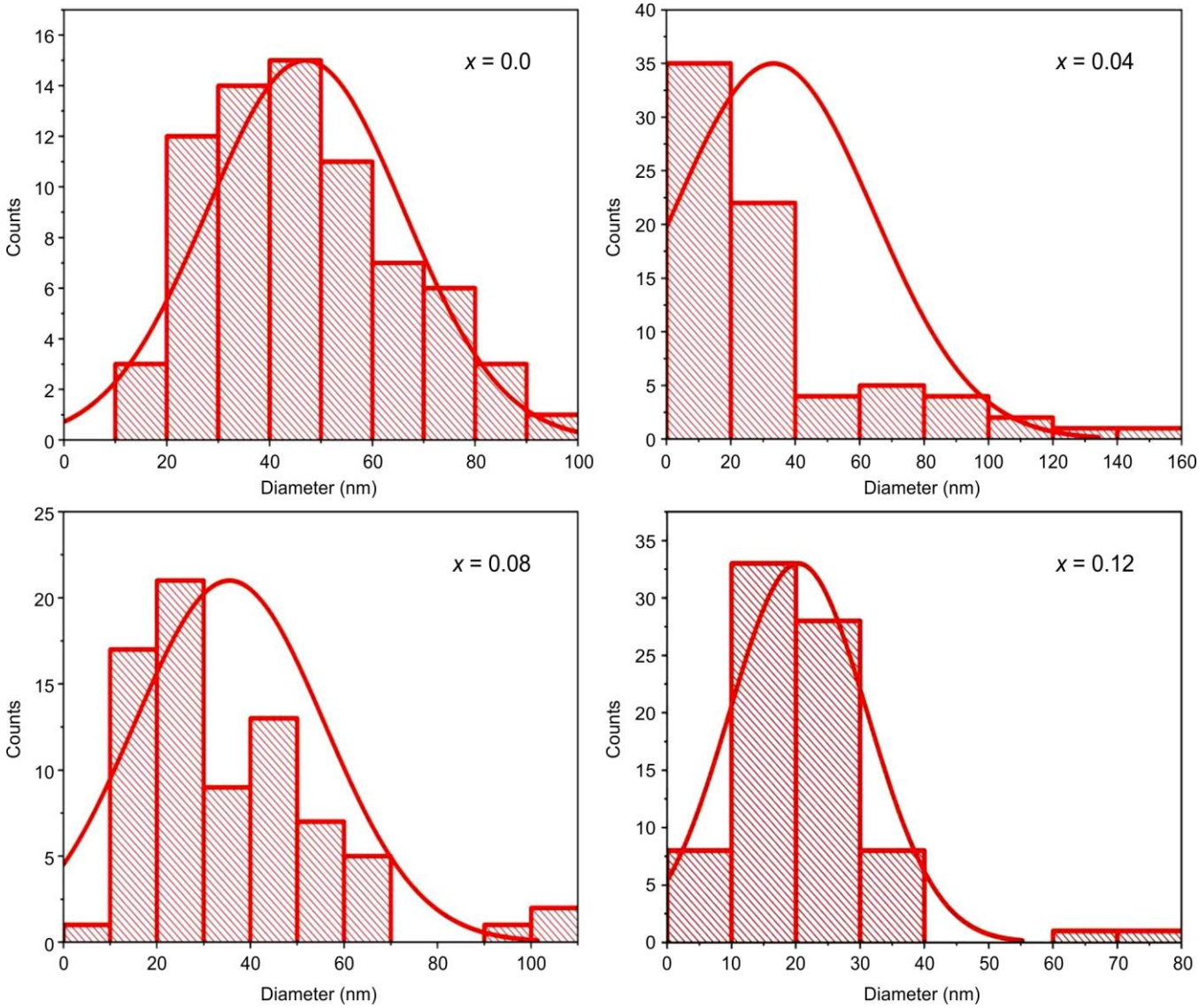

Fig. 4. Particle size distribution bar graphs of $Zn_{0.5}Mg_{0.5}Gd_xFe_{(2-x)}O_4$ (x = 0.0, 0.04, 0.08 and 0.12) ferrites

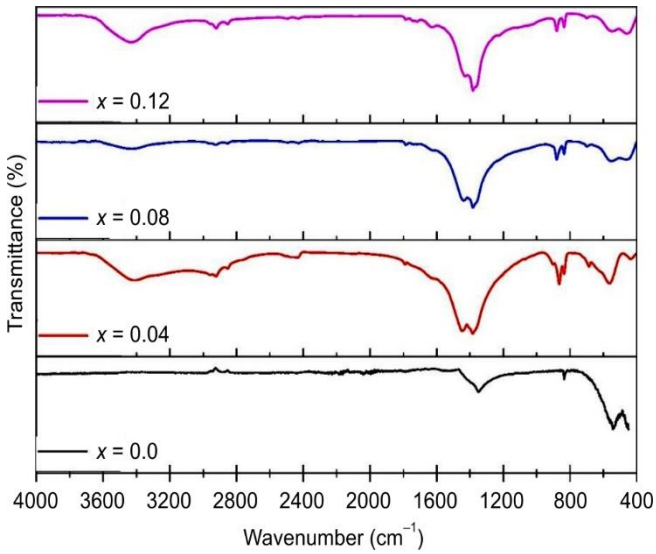

Fig. 5. FTIR spectra of $Zn_{0.5}Mg_{0.5}Gd_xFe_{(2-x)}O_4$ (x = 0.0, 0.04, 0.08 and 0.12) ferrites

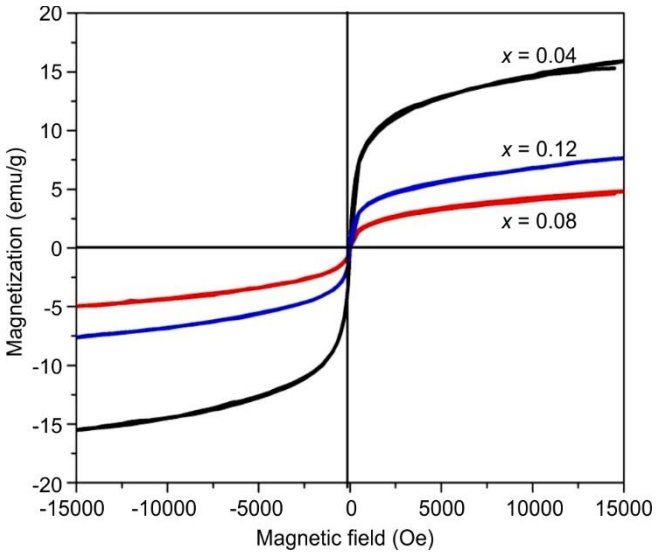

Fig. 6. Vibrating sample magnetometer curve of $Zn_{0.5}Mg_{0.5}Gd_xFe_{(2-x)}O_4$ (x = 0.0, 0.04, 0.08 and 0.12) ferrites

mately 3500 Oe, while the Gd_2 and Gd_1 samples had values of 2500 Oe and 2000 Oe, respectively. This indicates that the Gd_3 sample requires a stronger magnetic field to demagnetize compared to the other samples. The hysteresis loop area represents the energy loss per cycle during magnetization and demagnetization [33]. The Gd_3 sample also exhibited the largest hysteresis loop area, indicating the highest energy loss, followed by the Gd_2 and Gd_1 samples. This suggests that the Gd_3 sample may have higher losses in magnetic applications compared to the other samples. The parameter of vibrating sample magnetometer is showed in Table-2.

TABLE-2
THE PARAMETER OF VIBRATING SAMPLE MAGNETOMETER (VSM) FOR $Zn_{0.5}Mg_{0.5}Gd_xFe_{(2-x)}O_4$ (x = 0, 0.04, 0.08 AND 0.12) FERRITES

Parameter	x = 0.12	x = 0.08	x = 0.04
Saturation magnetization (emu/g)	~18	~12	~9
Remanent magnetization (emu/g)	~6	~4	~3
Coercivity (Oe)	~3500	~2500	~2000

Conclusion

In conclusion, this study conducted a synthesis of Gd^{3+} doped $Zn_{0.5}Mg_{0.5}Gd_xFe_{(2-x)}O_4$ ferrites, varying gadolinium content (x = 0.0, 0.04, 0.08 and 0.12) and extensively examined their structural and morphological characteristics. The analysis confirmed the presence of cubic spinel structures with *Fd*3*m* space group and tetragonal spinal structures in the Gd-doped ferrites, showcasing lattice constant variations that increased with Gd content up to x = 0.08 and then decreased. The expansion of lattice constant due to the substitution of larger Gd^{3+} ions for smaller Fe^{3+} ions was observed. SEM analysis showed that all samples exhibited spherical particle morphologies with crystallite sizes below 38 nm. The presence of non-uniformity and slight agglomeration is likely due to gas evolution during the synthesis process. FTIR spectroscopy confirmed the incorporation of metal ions and dopants through the identification of the characteristic absorption bands associated with metal–oxygen stretching vibrations. The magnetic parameters of saturation magnetization, remanent magnetization, coercivity and hysteresis loop area also provided valuable insights into the magnetic behaviour of materials. The differences observed in these parameters among the Gd_3, Gd_2 and Gd_1 samples highlight the importance of understanding and characterizing magnetic properties for various applications like in catalysis, sensors and magnetic technologies. The observed variations in lattice constants and structural features emphasize the need for tailored compositions in ferrites, presenting new avenues for future research and development in nanomaterials and their potential contributions to materials science, nanotechnology and advanced technological applications.

ACKNOWLEDGEMENTS

The authors would like thank to Jai Narain Vyas University Jodhpur (JNVU) for experimental facilities.

CONFLICT OF INTEREST

The authors declare that there is no conflict of interests regarding the publication of this article.

REFERENCES

1. T. Dippong, E.A. Levei and O. Cadar, *Nanomaterials*, **11**, 1560 (2021); https://doi.org/10.3390/nano11061560
2. A. Vedrtnam, K. Kalauni, S. Dubey, and A. Kumar, *AIMS Mater. Sci.*, **7**, 800 (2020); https://doi.org/10.3934/matersci.2020.6.800
3. T.N. Pham, T.Q. Huy and A.-T. Le, *RSC Adv.*, **10**, 31622 (2020); https://doi.org/10.1039/D0RA05133K
4. Sonia, H. Kumari, Suman, S. Chahal, S. Devi, S. Kumar, S. Kumar, P. Kumar and A. Kumar, *Appl. Phys., A Mater. Sci. Process.*, **129**, 91 (2023); https://doi.org/10.1007/s00339-022-06288-0
5. R. Valenzuela, *Phys. Res. Int.*, **2012**, e591839 (2012); https://doi.org/10.1155/2012/591839
6. A. Joseph and S. Mathew, *ChemPlusChem*, **79**, 1382 (2014); https://doi.org/10.1002/cplu.201402202
7. M. Souiyah, *Cogent Eng.*, **10**, 2172790 (2023); https://doi.org/10.1080/23311916.2023.2172790
8. G. Rana, P. Dhiman, A. Kumar, D.-V.N. Vo, G. Sharma, S. Sharma and M. Naushad, *Chem. Eng. Res. Des.*, **175**, 182 (2021); https://doi.org/10.1016/j.cherd.2021.08.040
9. M. Zulqarnain, S.S. Ali, C.H. Wan, U. Hira, A. Hussain and G. Farid, *Mater. Sci. Eng. B*, **298**, 116829 (2023); https://doi.org/10.1016/j.mseb.2023.116829
10. Y. Hadouch, D. Mezzane, M. Amjoud, L. Hajji, Y. Gagou, Z. Kutnjak, V. Laguta, Y. Kopelevich and M. El Marssi, *J. Magn. Magn. Mater.*, **563**, 169925 (2022); https://doi.org/10.1016/j.jmmm.2022.169925
11. K.R. Sanchez-Lievanos, J.L. Stair and K.E. Knowles, *Inorg. Chem.*, **60**, 4291 (2021); https://doi.org/10.1021/acs.inorgchem.1c00040
12. S.R. Mokhosi, W. Mdlalose, S. Mngadi, M. Singh and T. Moyo, *J. Phys. Conf. Ser.*, **1310**, 012014 (2019); https://doi.org/10.1088/1742-6596/1310/1/012014
13. H.J. Kardile, S.B. Somvanshi, A.R. Chavan, A.A. Pandit and K.M. Jadhav, *Optik*, **207**, 164462 (2020); https://doi.org/10.1016/j.ijleo.2020.164462
14. S.J. Salih and W.M. Mahmood, *Heliyon*, **9**, e16601 (2023); https://doi.org/10.1016/j.heliyon.2023.e16601
15. S.N. Patil, A.M. Pawar, S.K. Tilekar and B.P. Ladgaonkar, *Sens. Actuators A Phys.*, **244**, 35 (2016); https://doi.org/10.1016/j.sna.2016.04.019
16. S. Laurent, S. Dutz, U.O. Häfeli and M. Mahmoudi, *Adv. Colloid Interface Sci.*, **166**, 8 (2011); https://doi.org/10.1016/j.cis.2011.04.003
17. Y. Kumar, S. Chopra, A. Gupta, Y. Kumar, S.J. Uke and S.P. Mardikar, *Mater. Sci. Energy Technol.*, **3**, 566 (2020); https://doi.org/10.1016/j.mset.2020.06.002
18. Y. Kumar, A. Gupta, A.K. Thakur, S.J. Uke, V. Khatri, A. Kumar, M. Gupta and Y. Kumar, *J. Nanopart. Res.*, **23**, 119 (2021); https://doi.org/10.1007/s11051-021-05221-5
19. M. Hassan, Y. Slimani, M.A. Gondal, M.J.S. Mohamed, S. Güner, M.A. Almessiere, A.M. Surrati, A. Baykal, S. Trukhanov and A. Trukhanov, *Ceram. Int.*, **48**, 24866 (2022); https://doi.org/10.1016/j.ceramint.2022.05.140
20. M.A. Almessiere, B. Ünal, S. Ali, A. Baykal, Y. Slimani and A.V. Trukhanov, *Ceram. Int.*, **48**, 25390 (2022); https://doi.org/10.1016/j.ceramint.2022.05.214
21. M. Aadil, A.G. Taki, S. Zulfiqar, A. Rahman, M. Shahid, M.F. Warsi, Z. Ahmad, A.A. Alothman and S. Mohammad, *RSC Adv.*, **13**, 28063 (2023); https://doi.org/10.1039/D3RA05290G
22. E. AlArfaj, S. Hcini, A. Mallah, M.H. Dhaou and M.L. Bouazizi, *J. Supercond. Nov. Magn.*, **31**, 4107 (2018); https://doi.org/10.1007/s10948-018-4694-8
23. M. Mustaqeem, K. Mahmood, T.A. Saleh, A. Rehman, M. Ahmad, Z.A. Gilani and M. Asif, *Physica B*, **588**, 412176 (2020); https://doi.org/10.1016/j.physb.2020.412176
24. V. Manikandan, A. Vanitha, E. Ranjith Kumar and J. Chandrasekaran, *J. Magn. Magn. Mater.*, **423**, 250 (2017); https://doi.org/10.1016/j.jmmm.2016.09.077

25. X. Yu, R. Yang, C. Wu, B. Liu and W. Zhang, *Magnetochemistry*, **9**, 181 (2023); https://doi.org/10.3390/magnetochemistry9070181
26. A. Komal, A. Kumar, Y. Kumar and V.K. Shukla, *J. Mater. Sci. Mater. Electron.*, **34**, 1880 (2023); https://doi.org/10.1007/s10854-023-11309-6
27. Q. Lin, J. Lin, Y. He, R. Wang and J. Dong, *J. Nanomater.*, **2015**, e294239 (2015); https://doi.org/10.1155/2015/294239
28. S. Ram and S. Singh, *World J. Chem. Educ.*, **10**, 76 (2022); https://doi.org/10.12691/wjce-10-2-4
29. F. Siadatnasab, S. Farhadi, A.-A. Hoseini and M. Sillanpää, *New J. Chem.*, **44**, 16234 (2020); https://doi.org/10.1039/D0NJ03441J
30. F. da S. Duarte, A.L.M.S. Melo, A.B. Ferro, C.L.P.S. Zanta, J.L.S. Duarte and R.M.P.B. Oliveira, *Materials*, **15**, 8185 (2022); https://doi.org/10.3390/ma15228185
31. M. Lenglet, *Active Passive Elect. Comp.*, **27**, 1 (2004); https://doi.org/10.1080/0882751031000116142
32. D.R. Kumar, S.I. Ahmad, C.A. Lincoln and D. Ravinder, *J. Asian Ceram. Soc.*, **7**, 53 (2019); https://doi.org/10.1080/21870764.2018.1563036
33. A.I. Ahmed, M.A. Siddig, A.A. Mirghni, M.I. Omer and A.A. Elbadaw, *Adv. Nanopart.*, **4**, 35 (2015); https://doi.org/10.4236/anp.2015.42006